

PAPER

Balancing fluorescence and singlet oxygen formation in push–pull type near-infrared BODIPY photosensitizers†

Jasper Deckers,^{id} ‡^{abc} Tom Cardeynaels,^{id} ‡^{abcd} Sandra Doria,^{ef} Nikolay Tumanov,^{id} ^g Andrea Lapini,^{eh} Anitha Ethirajan,^{id} ^{bi} Marcel Ameloot,^{id} ^j Johan Wouters,^g Mariangela Di Donato,^{id} ^{ef} Benoît Champagne^{id} ^d and Wouter Maes^{id} ^{*abc}

Boron dipyrromethene dyes are highly attractive for image-guided photodynamic therapy. Nevertheless, their clinical breakthrough as theranostic agents is still obstructed by several limitations. Here, we report a series of strongly absorbing, heavy-atom-free, distyryl-BODIPY donor–acceptor dyads operating within the phototherapeutic window. Whereas diphenylamine and carbazole donors lead to strong fluorescence, dimethylacridine, phenoxazine, and phenothiazine units afford a decent fluorescence combined with the efficient formation of singlet oxygen. Dedicated photophysical analysis and quantum-chemical calculations are performed to elucidate the excited state dynamics responsible for the pronounced differences within the BODIPY series. Femtosecond transient absorption spectra reveal the nature of the excited state processes and the involvement of charge-transfer states in triplet formation.

Received 13th April 2022,
Accepted 6th June 2022

DOI: 10.1039/d2tc01526a

rsc.li/materials-c

Introduction

Singlet oxygen (denoted as $O_2(^1\Delta_g)$, shortened as 1O_2) is a powerful reagent that is employed in the manufacture of fine chemicals, wastewater treatment, blood sterilization, and the production of specific insecticides and herbicides, among others.¹ Furthermore, the combination of its high reactivity, related short lifetime, and slow diffusion rate in biological media, renders 1O_2 the protagonist in photodynamic therapy (PDT).^{2,3} In PDT, light is used to activate a photosensitizer (PS), which then produces reactive oxygen species (ROS) through different mechanisms.⁴ These ROS result in the selective destruction of tumor cells at the irradiation site, allowing PDT to be used for cancer therapy. Furthermore, PDT can also be employed in a broader sense for treating ophthalmic and dermatologic diseases, bacterial and fungal infections, and the inactivation of viruses.^{5–12} Whereas type I PDT investigates ROS formation upon direct interaction of the activated PS with a substrate, most studies focus on the type II PDT process since 1O_2 is considered the leading cytotoxic agent.¹³ In more detail, the PS is excited with photons of a suitable wavelength, thereby achieving an electronically excited singlet state (S_n). For 1O_2 formation, intersystem crossing (ISC) is required to obtain a triplet state (T_n) from which, after fast internal conversion to the first triplet state (T_1), energy transfer to molecular oxygen ($O_2(^3\Sigma_g^-)$ or 3O_2) can occur.¹⁴ As ISC is a spin-forbidden

^a UHasselt – Hasselt University, Institute for Materials Research (IMO), Design & Synthesis of Organic Semiconductors (DSOS), Agoralaan, 3590 Diepenbeek, Belgium. E-mail: wouter.maes@uhasselt.be

^b IMEC, Associated Lab IMOMEC, Wetenschapspark 1, 3590 Diepenbeek, Belgium

^c Energyville, Thorpark, 3600 Genk, Belgium

^d UNamur – University of Namur, Namur Institute of Structured Matter, Theoretical and Structural Physical Chemistry Unit, Laboratory of Theoretical Chemistry (LTC), Rue de Bruxelles 61, 5000 Namur, Belgium

^e European Laboratory for Non-Linear Spectroscopy (LENS), Via Nello Carrara 1, 50019 Sesto Fiorentino (FI), Italy

^f Istituto di Chimica dei Composti OrganoMetallici (ICCOM-CNR), Via Madonna Del Piano 10, 50019 Sesto Fiorentino (FI), Italy

^g UNamur – University of Namur, Namur Medicine and Drug Innovation Center (NAMEDIC), Namur Research Institute for Life Sciences (NARILIS), Namur Institute of Structured Matter (NISM), Rue de Bruxelles 61, 5000 Namur, Belgium

^h Department of Chemistry, Life Science and Environmental Sustainability, University of Parma, Parco Area delle Scienze, 17/A, 43124 Parma, Italy

ⁱ UHasselt – Hasselt University, Institute for Materials Research (IMO), Nano-Biophysics and Soft Matter Interfaces (NSI), Wetenschapspark 1, 3590 Diepenbeek, Belgium

^j UHasselt – Hasselt University, Biomedical Research Institute (BIOMED), Agoralaan, 3590 Diepenbeek, Belgium

† Electronic supplementary information (ESI) available: Materials and methods, detailed BODIPY dyad synthesis procedures and characterization data, additional (TD)DFT data and figures, single-crystal X-ray structures, singlet oxygen generation plots, additional absorption and emission spectra and data, additional transient absorption spectra and data, and $^1H/^{13}C$ NMR spectra can be found. CCDC 2122792–2122794. For ESI and crystallographic data in CIF or other electronic format see DOI: <https://doi.org/10.1039/d2tc01526a>

‡ These authors contributed equally.

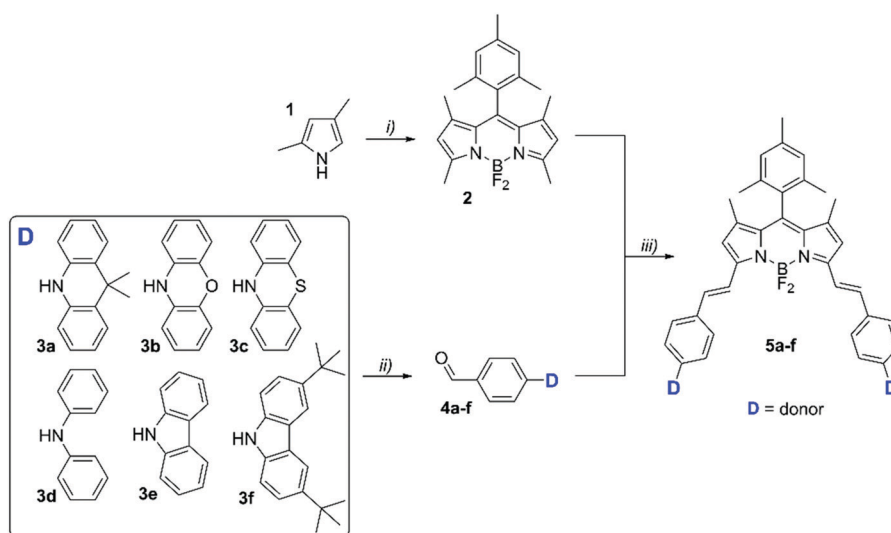
1 transition, the quest for compounds with efficient triplet
2 formation remains a crucial research topic.

3 Throughout the years, a vast amount of organic photosensi-
4 tizers have been reported.^{15–23} Among these promising mole-
5 cules, 4,4-difluoro-4-bora-3a,4a-diaza-s-indacenes (commonly
6 indicated as boron dipyrromethenes or BODIPYs) are one of
7 the most prominent examples.^{24–36} Their high molar extinction
8 coefficients, (photo)chemical stability, and easily tunable
9 photophysical properties make them attractive PSs.^{37–39} How-
10 ever, typically high fluorescence quantum yields (Φ_f) of BODIPY
11 dyes imply ISC restrictions as these are competing decay
12 processes for the first singlet excited state. The most encoun-
13 tered solution is the introduction of bromine, iodine, or
14 transition metal complexes on the BODIPY structure, thereby
15 increasing spin–orbit coupling (SOC) through the so-called
16 heavy-atom effect.^{40–43} Nevertheless, related additional syn-
17 thetic efforts and costs, shortened triplet state lifetimes, low
18 photostability, and increased dark cytotoxicity provided an
19 impetus to search for alternative ISC mechanisms.^{44–46} In this
20 way, novel BODIPY PSs were developed, based on reduced
21 singlet–triplet energy gaps (ΔE_{ST}), spin converters, radical-
22 enhanced ISC, radical pair ISC, twisted π -conjugation-induced
23 ISC, and spin–orbit charge-transfer ISC (SOCT-ISC).^{40–42,47,48}
24 These alternative approaches open the possibility for theranos-
25 tic applications as subtle engineering of the energy levels can
26 allow triplet population and singlet emission to coexist. In PDT,
27 these self-reporting PSs present an appealing step toward
28 personalized cancer treatment, enabling the combination of
29 diagnosis and therapy to localize the target, monitor the
30 therapeutic progression, and improve drug dosimetry.^{49–51}

31 Another essential feature for PDT PSs is their activity in the
32 near-infrared (NIR) spectral region. Shorter wavelengths are
33 more prone to scattering and several tissue chromophores will

34 filter the UV-VIS part of the incoming light.^{14,52,53} Wavelengths
35 between 600 and 800 nm are desired to limit light scattering,
36 reduce background signals, and enhance tissue penetration
37 depths.⁵⁴ Although strategies to bathochromically shift the
38 absorption and emission properties are well-known for BODIPY
39 dyes, it is not straightforward to combine strong $^1\text{O}_2$ production
40 with a decent brightness in the phototherapeutic region.^{55–58}
41 Hence, only a handful of NIR-photoactive heavy-atom-free dual-
42 functioning BODIPY PSs have been developed so far.^{59–66}

43 Recently, we reported a series of distyryl–BODIPY–acridine
44 dyads, active in the phototherapeutic window, showing
45 balanced brightness and phototoxic power.⁶⁶ Concentration-
46 dependent fluorescence experiments suggested the involve-
47 ment of ‘exciplex’⁶⁷ energy states in the decay mechanism.
48 Relatively long exciplex state lifetimes, combined with their
49 polar nature, would render them a suitable intermediate in the
50 ISC process, as previously reported for other donor–acceptor
51 BODIPY systems.^{68–70} To gain more insights into the relation-
52 ship between the molecular structure and the photophysical
53 properties of distyryl–BODIPY dyads, we report here on the
54 development of a new series of donor–acceptor type BODIPY
55 dyads wherein the electron donor moieties are varied. Diphe-
56 nylamine and carbazole donors were found to afford high
57 fluorescence quantum yields ($\Phi_f \sim 45$ –75%) in polar and
58 apolar solutions. However, negligible $^1\text{O}_2$ formation was
59 observed for these systems. In line with our previous results
60 for dimethylacridine, incorporation of phenoxazine and phe-
61 nothiazine donors resulted in efficient PSs, with $^1\text{O}_2$ quantum
62 yields (Φ_Δ) ranging from 33 to 47% in both chloroform and
63 toluene solution. Fluorescence emission was quenched in
64 chloroform for these dyads, but this feature was retained in
65 toluene, resulting in Φ_f values around 50%. Hence, these
66 distyryl–BODIPY dyads are interesting self-reporting PDT PSs.



35
36
37
38
39
40
41
42
43
44
45
46
47
48
49
50
51
52
53
54
55
56
57
58
59
60
61
62
63
64
65
66
67
68
69
70
71
72
73
74
75
76
77
78
79
80
81
82
83
84
85
86
87
88
89
90
91
92
93
94
95
96
97
98
99
100
101
102
103
104
105
106
107
108
109
110
111
112
113
114
115
116
117
118
119
120
121
122
123
124
125
126
127
128
129
130
131
132
133
134
135
136
137
138
139
140
141
142
143
144
145
146
147
148
149
150
151
152
153
154
155
156
157
158
159
160
161
162
163
164
165
166
167
168
169
170
171
172
173
174
175
176
177
178
179
180
181
182
183
184
185
186
187
188
189
190
191
192
193
194
195
196
197
198
199
200
201
202
203
204
205
206
207
208
209
210
211
212
213
214
215
216
217
218
219
220
221
222
223
224
225
226
227
228
229
230
231
232
233
234
235
236
237
238
239
240
241
242
243
244
245
246
247
248
249
250
251
252
253
254
255
256
257
258
259
260
261
262
263
264
265
266
267
268
269
270
271
272
273
274
275
276
277
278
279
280
281
282
283
284
285
286
287
288
289
290
291
292
293
294
295
296
297
298
299
300
301
302
303
304
305
306
307
308
309
310
311
312
313
314
315
316
317
318
319
320
321
322
323
324
325
326
327
328
329
330
331
332
333
334
335
336
337
338
339
340
341
342
343
344
345
346
347
348
349
350
351
352
353
354
355
356
357
358
359
360
361
362
363
364
365
366
367
368
369
370
371
372
373
374
375
376
377
378
379
380
381
382
383
384
385
386
387
388
389
390
391
392
393
394
395
396
397
398
399
400
401
402
403
404
405
406
407
408
409
410
411
412
413
414
415
416
417
418
419
420
421
422
423
424
425
426
427
428
429
430
431
432
433
434
435
436
437
438
439
440
441
442
443
444
445
446
447
448
449
450
451
452
453
454
455
456
457
458
459
460
461
462
463
464
465
466
467
468
469
470
471
472
473
474
475
476
477
478
479
480
481
482
483
484
485
486
487
488
489
490
491
492
493
494
495
496
497
498
499
500
501
502
503
504
505
506
507
508
509
510
511
512
513
514
515
516
517
518
519
520
521
522
523
524
525
526
527
528
529
530
531
532
533
534
535
536
537
538
539
540
541
542
543
544
545
546
547
548
549
550
551
552
553
554
555
556
557
558
559
560
561
562
563
564
565
566
567
568
569
570
571
572
573
574
575
576
577
578
579
580
581
582
583
584
585
586
587
588
589
590
591
592
593
594
595
596
597
598
599
600
601
602
603
604
605
606
607
608
609
610
611
612
613
614
615
616
617
618
619
620
621
622
623
624
625
626
627
628
629
630
631
632
633
634
635
636
637
638
639
640
641
642
643
644
645
646
647
648
649
650
651
652
653
654
655
656
657
658
659
660
661
662
663
664
665
666
667
668
669
670
671
672
673
674
675
676
677
678
679
680
681
682
683
684
685
686
687
688
689
690
691
692
693
694
695
696
697
698
699
700
701
702
703
704
705
706
707
708
709
710
711
712
713
714
715
716
717
718
719
720
721
722
723
724
725
726
727
728
729
730
731
732
733
734
735
736
737
738
739
740
741
742
743
744
745
746
747
748
749
750
751
752
753
754
755
756
757
758
759
760
761
762
763
764
765
766
767
768
769
770
771
772
773
774
775
776
777
778
779
780
781
782
783
784
785
786
787
788
789
790
791
792
793
794
795
796
797
798
799
800
801
802
803
804
805
806
807
808
809
810
811
812
813
814
815
816
817
818
819
820
821
822
823
824
825
826
827
828
829
830
831
832
833
834
835
836
837
838
839
840
841
842
843
844
845
846
847
848
849
850
851
852
853
854
855
856
857
858
859
860
861
862
863
864
865
866
867
868
869
870
871
872
873
874
875
876
877
878
879
880
881
882
883
884
885
886
887
888
889
890
891
892
893
894
895
896
897
898
899
900
901
902
903
904
905
906
907
908
909
910
911
912
913
914
915
916
917
918
919
920
921
922
923
924
925
926
927
928
929
930
931
932
933
934
935
936
937
938
939
940
941
942
943
944
945
946
947
948
949
950
951
952
953
954
955
956
957
958
959
960
961
962
963
964
965
966
967
968
969
970
971
972
973
974
975
976
977
978
979
980
981
982
983
984
985
986
987
988
989
990
991
992
993
994
995
996
997
998
999
1000

1 Femtosecond transient absorption spectroscopy (fs-TAS) was used to gain detailed insights in the excited state processes, suggesting the involvement of charge-transfer (CT) states in the ultrafast dynamics.

Results and discussion

Photosensitizer design and synthesis

10 The molecular design of the newly developed systems was inspired on the recently reported distyryl-BODIPY-acridine donor-acceptor (D-A) dyad **5a**, possessing both an attractive brightness and phototoxicity within the phototherapeutic window.⁶⁶ The donor end group (dimethylacridine **3a**) was deemed essential to realize exciplex formation and to allow for efficient ISC to occur. To further elucidate the origin of the ISC and the influence of the molecular design on this process, a variety of alternative donor units were now screened, going from phenoxazine (**3b**) to phenothiazine (**3c**), diphenylamine (**3d**), carbazole (**3e**), and 3,6-di-*tert*-butylcarbazole (**3f**) (Scheme 1).

For the material synthesis, donor moieties **3a-f** were first combined with 4-bromobenzaldehyde in a Buchwald-Hartwig amination reaction using tris(dibenzylideneacetone)dipalladium(0) ($\text{Pd}_2(\text{dba})_3$) and 1,1'-bis(diphenylphosphino)ferrocene (dppf) as the catalytic system to yield aldehydes **4a-f** in moderate to high yields (59–92%). The highly fluorescent 1,3,5,7-tetramethyl-BODIPY core **2** was obtained from 2,4-dimethylpyrrole (**1**) according to a literature procedure.⁷¹ This *meso*-methyl-BODIPY structure was chosen for its facile synthesis and good solubility of the resulting BODIPY dyads. The relatively acidic protons of the α -methyl groups enable a Knoevenagel-type condensation to afford the desired distyryl-BODIPY dyads **5a-f**. A short and easy synthetic procedure, comprising five-minute microwave irradiation in the presence of glacial acetic acid and piperidine, resulted in good to high yields (54–91%). The reaction conditions were optimized previously for dimethylacridine **3a**.⁶⁶ For a detailed description of the synthesis protocols and material characterization data, we refer to the ESI.[†]

Structural analysis

45 Density functional theory (DFT) calculations were performed to analyze the molecular structures of the BODIPY dyads with varying donor units. All geometries were optimized using the M06-2X exchange-correlation functional with the 6-311G(d) basis set and the polarizable continuum model (PCM) to simulate the moderately polar environment of a chloroform solution. Vibrational analysis was performed to confirm that all geometries correspond to minima on the potential energy surfaces. By varying the attached donor end groups in the distyryl-BODIPY dyads, large differences in the dihedral angles between the donor and acceptor moieties were observed, ranging from 34° for the diphenylamine unit (**5d**) to 90° for dimethylacridine, phenoxazine, and phenothiazine (**5a-c**) (Fig. 1). This torsion angle is the same for both arms. All donor

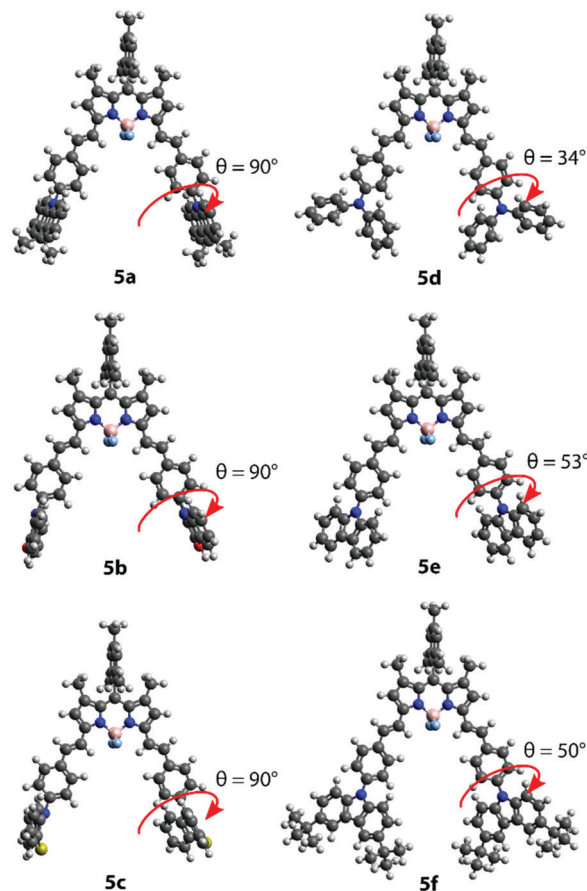


Fig. 1 Optimized ground-state geometries for BODIPYs **5a-f** with the dihedral angles between the donor units and the distyryl-BODIPY core indicated by red arrows.

units are planar, with the exception of phenothiazine (**5c**), which is bent with an angle of 33°, and diphenylamine (**5d**), which has an angle of 70° between the two phenyl rings. The frontier molecular orbitals (Fig. S1 and S2, ESI[†]) show that the highest occupied molecular orbital (HOMO) and the lowest unoccupied molecular orbital (LUMO) are located on the distyryl-BODIPY unit for **5a-f**, except for the HOMO orbital of **5b**, which is located on one of the phenoxazine units. The HOMO-1 and HOMO-2 orbitals are mainly localized on the respective donor units, again except for BODIPY **5b**, for which the HOMO-2 orbitals are located on the distyryl-BODIPY core. This discrepancy for **5b** can be explained by considering the energy levels of the various orbitals (Table S1, ESI[†]). The quasi-degenerate HOMO-2, HOMO-1, and HOMO energies are within 0.05 eV from each other, allowing an inversion between the character of HOMO/HOMO-1 (both localized on the donor unit) and HOMO-2 (localized on the styryl-BODIPY moiety).⁷² The smaller dihedral angles in BODIPYs **5d-f** lead to increased HOMO delocalization toward the donor unit (Fig. S2, ESI[†]). In all compounds, the *meso*-methyl group is nearly perpendicular to the rest of the BODIPY core, electronically decoupled from it.

Single crystals were obtained for BODIPYs **5a**, **5c**, and **5e** (Fig. S3-S5 and Table S2, ESI[†]). The single-crystal X-ray

structures confirm the molecular structures of the designed BODIPY units and also indicate that the correct geometrical conformations are probed for the time-dependent DFT (TDDFT) calculations (*vide infra*). In addition, the dihedral angles between the donor and acceptor groups were found to be 89° for **5a**, 80° for **5c**, and 70° for **5e**, which is in good agreement with the DFT calculations (Fig. 1). In contrast to the findings of the DFT geometry optimization, the dimethylacridine unit is slightly bent (14°) in the single crystal structure. The bending of phenothiazine is 21° in the crystal structure, which is slightly less than observed in the geometry optimization.

TDDFT calculations

To assess the optical properties of BODIPY dyads **5a–f**, TDDFT calculations were performed using M06-2X as the exchange-correlation functional and 6-311G(d) as the basis set. The PCM was applied to simulate the solution measurement conditions in chloroform. The lowest singlet vertical excitation energies for **5a–f** are all in the region of 2.01–2.16 eV (617–573 nm) (Table 1). The second singlet vertical excitation energies are considerably larger ($\Delta E_{S_1-S_2} = 0.85\text{--}1.20$ eV), making it unlikely that the S_2 states play a significant role in the photophysical properties. The two lowest triplet vertical excitation energies vary from 1.15–1.20 eV and 2.30–2.56 eV, respectively. This means that the first singlet vertical excitation energy is in between the two first triplet vertical excitation energies in all cases, as previously observed for the dimethylacridine-containing dyad **5a**.⁶⁶ BODIPY dyads **5d–f** show slightly lower first singlet and first triplet vertical excitation energies with respect to BODIPYs **5a–c**. This is likely due to the smaller dihedral angles for these donor units, resulting in delocalization of the HOMO from the BODIPY part onto the donor unit, which is not seen for BODIPYs **5a–c** (Fig. S1 and S2, ESI†). The increase in HOMO delocalization gives rise to a more extended π -conjugated system for the transition as the first singlet excited state is of HOMO \rightarrow LUMO character for all dyads, except for **5b** (HOMO–2 \rightarrow LUMO), for which we already denoted the inversion between the HOMO and HOMO–2 orbitals. The first singlet excited

state has a large oscillator strength, which indicates high molar absorptivities (*i.e.* strong absorption).

To probe the CT characteristics of the push–pull BODIPY series, the ground and excited state electron densities were evaluated according to the work of Le Bahers *et al.*, using the distance over which charge is transferred (d_{CT}) and the change in dipole moment ($\Delta\mu$) as figures of merit (Table 2).⁷³ As the name implies, excitations with a higher degree of CT character will have larger values for d_{CT} since the charge is transferred over a certain distance as opposed to localized excitations in which the charge is merely redistributed over a given part of the molecule. Furthermore, CT excitations are characterized by a more significant $\Delta\mu$ as the charge is transferred from one part of the molecule to the other, creating areas with reduced and increased charge density distributions. For dyads **5a–f**, the $S_0 \rightarrow S_2$ transition seems to be the only excitation with CT character, as indicated by the relatively large d_{CT} (≥ 4.22 Å) and $\Delta\mu$ (≥ 18.4 D) values with respect to those for the other transitions (≤ 2.71 Å for d_{CT} and ≤ 7.2 D for $\Delta\mu$) (Table 2). As discussed before, the vertical excitation energy for the $S_0 \rightarrow S_2$ transition is much higher than for $S_0 \rightarrow S_1$ (Table 1). Hence, it seems unlikely that the S_2 state plays a significant role in the ISC process. These findings can also be visualized by considering the difference between the excited and ground state electron densities, as shown in Fig. S6 and S7 (ESI†).

Photophysical characterization

The photophysical properties of the six distyryl–BODIPY dyads **5a–f** were investigated in a relatively polar (*i.e.* chloroform) and rather apolar (*i.e.* toluene) medium to explore their absorption and fluorescence behavior and their ability to generate 1O_2 . Absorption and emission spectra afforded the basic spectral data (Fig. 2 and Table 3). Φ_f values were obtained at an excitation wavelength of 605 nm, relative to Nile blue. Φ_Δ data were collected by monitoring the absorbance of 1,3-diphenylisobenzofuran (1,3-DPBF) as a 1O_2 scavenger upon excitation at 639 nm (Fig. S8, ESI†). In combination with the molar attenuation coefficients (ϵ), the brightness (BT) and phototoxic power (PP) were determined. All data reported in

Table 1 Calculated vertical singlet (S_1 and S_2) and triplet (T_1 and T_2) excitation energies and their corresponding oscillator strengths for BODIPYs **5a–f**. The dominant nature of the one-particle excitations is also given

BODIPY	$S_0 \rightarrow S_1$			$S_0 \rightarrow S_2$			$S_0 \rightarrow T_1$		$S_0 \rightarrow T_2$	
	ΔE^a (eV)	Osc. Str. ^b	Nature ^c	ΔE^a (eV)	Osc. Str. ^b	Nature ^c	ΔE^a (eV)	Nature ^c	ΔE^a (eV)	Nature ^c
5a	2.16 (574 nm)	1.20	H \rightarrow L (97%)	3.08	0.00	H–1 \rightarrow L (85%)	1.20	H \rightarrow L (93%)	2.55	H–3 \rightarrow L (50%)
5b	2.16 (573 nm)	1.19	H–2 \rightarrow L (96%)	3.01	0.00	H \rightarrow L (89%)	1.20	H–2 \rightarrow L (93%)	2.56	H–3 \rightarrow L (49%)
5c	2.16 (573 nm)	1.19	H \rightarrow L (97%)	3.27	0.00	H–1 \rightarrow L (91%)	1.20	H \rightarrow L (94%)	2.55	H–5 \rightarrow L (50%)
5d	2.01 (617 nm)	1.27	H \rightarrow L (90%)	2.97	1.65	H–1 \rightarrow L (85%)	1.15	H \rightarrow L (78%)	2.30	H–1 \rightarrow L (45%)
5e	2.12 (585 nm)	1.24	H \rightarrow L (93%)	3.32	1.53	H–1 \rightarrow L (77%)	1.19	H \rightarrow L (86%)	2.49	H–5 \rightarrow L (32%)
5f	2.11 (589 nm)	1.23	H \rightarrow L (89%)	3.20	1.37	H–1 \rightarrow L (81%)	1.18	H \rightarrow L (80%)	2.47	H–5 \rightarrow L (33%)

^a Vertical excitation energy/wavelength. ^b Oscillator strength. ^c H = HOMO, L = LUMO.

1 **Table 2** Amount of charge-transfer character (d_{CT}) and change in dipole moment ($\Delta\mu$, excited state dipole – ground state dipole) accompanying the $S_0 \rightarrow S_n$ and $S_0 \rightarrow T_n$ ($n = 1, 2$) transitions in chloroform

BODIPY	$S_0 \rightarrow S_1$		$S_0 \rightarrow S_2$		$S_0 \rightarrow T_1$		$S_0 \rightarrow T_2$	
	d_{CT}^a (Å)	$\Delta\mu^b$ (D)	d_{CT}^a (Å)	$\Delta\mu^b$ (D)	d_{CT}^a (Å)	$\Delta\mu^b$ (D)	d_{CT}^a (Å)	$\Delta\mu^b$ (D)
5a	0.64	1.3	5.14	34.7	0.64	1.7	0.38	0.6
5b	0.66	1.3	6.17	42.6	0.70	1.9	0.33	0.5
5c	0.59	1.2	6.11	41.8	0.64	1.7	0.28	0.5
5d	2.09	5.3	4.22	18.4	1.02	2.9	2.71	7.2
5e	1.17	2.5	4.61	20.2	0.75	2.0	1.48	2.9
5f	1.41	3.1	4.81	23.9	0.81	2.2	1.96	4.1

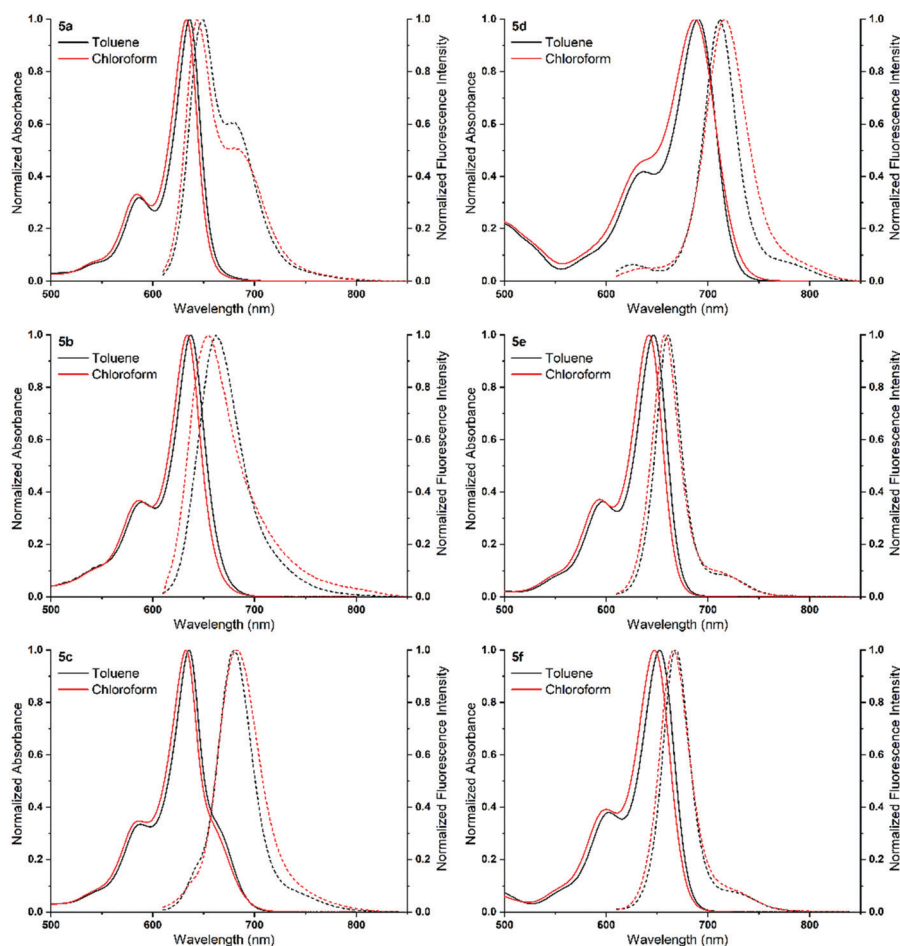
^a Distance over which charge is transferred between the indicated states upon excitation. ^b Change in dipole moment upon excitation.

15 Table 3 are mean values from three independent measurements for each compound in the indicated solvent. Only data from the wavelength region of interest are displayed here. For the full absorption spectra, we refer to Fig. S9 and Table S3 (ESI†).

20 For all BODIPY dyes, absorption maxima in chloroform were found above 630 nm, within the phototherapeutic window. Dyad 5d, carrying the diphenylamine donor, afforded the

largest bathochromic shift (190 nm) with respect to the initial BODIPY core 2, with an absorption maximum around 690 nm. The relative positions of the absorption maxima of the different materials nicely reflect the trends in the calculated S_1 energies (Table 1). The absorption profiles resemble these of typical BODIPY dyes as they are sharp and have a high-energy absorption shoulder. The phenothiazine and diphenylamine-functionalized dyads have slightly different spectra. BODIPY 5c shows a second, red-shifted shoulder, while the absorption band of BODIPY 5d is clearly broadened. In the UV region, an absorption peak around 350 nm is observed in all cases, originating from the distyryl extension of the BODIPY core (Fig. S9 and Table S3, ESI†). Other UV peaks are related to the incorporated donor. Absorption profiles in toluene solution almost entirely coincide with those in chloroform, although being slightly red-shifted (~ 4 nm).

As it is known that phenothiazine units can afford dual stable conformers, a relaxed potential energy surface scan was performed for compound 5c using the M06-2X/6-311G(d) method (Fig. S10, ESI†).⁷⁴ This revealed the existence of a slightly more stable conformer wherein one phenothiazine donor unit has a much smaller dihedral angle with the distyryl



35 **Fig. 2** Normalized absorption spectra (solid lines) for BODIPYs 5a–f and their corresponding normalized fluorescence emission spectra (dashed lines; $\lambda_{exc} = 605$ nm) in toluene and chloroform.

1 Table 3 Spectroscopic data for BODIPY dyads **5a–f** as obtained in toluene and chloroform solution^a

BODIPY	Solv. ^b	λ_{abs}^c (nm)	λ_{em}^d (nm)	$\Delta\nu^e$ (cm ⁻¹)	fwhm _{abs} ^f (cm ⁻¹)	fwhm _{em} ^g (cm ⁻¹)	ϵ^h (M ⁻¹ cm ⁻¹)	Φ_f^i	Φ_{Δ}^j	BT ^k (M ⁻¹ cm ⁻¹)	PP (M ⁻¹ cm ⁻¹) ^l
5a	TOL	636	649	323	744	1333	1.24×10^5	0.69 ± 0.03	0.07 ± 0.01	86 200	9000
	CL	633	645	294	777	917	1.20×10^5	0.63 ± 0.03	0.23 ± 0.02	75 200	27 000
5b	TOL	638	663	592	884	1086	1.05×10^5	0.47 ± 0.00	0.47 ± 0.03	49 200	49 900
	CL	634	653	459	882	1165	9.48×10^4	<0.01	0.37 ± 0.02	400	35 100
5c	TOL	636	680	1017	867	777	1.12×10^5	0.53 ± 0.00	0.33 ± 0.01	59 600	36 900
	CL	633	683	1156	913	987	1.00×10^5	0.05 ± 0.00	0.38 ± 0.01	5500	37 900
5d	TOL	691	712	427	1033	729	1.06×10^5	0.47 ± 0.01	0.06 ± 0.01	49 700	6300
	CL	687	716	589	1304	916	9.63×10^4	0.43 ± 0.00	0.06 ± 0.00	40 900	5600
5e	TOL	647	661	339	858	659	1.16×10^5	0.73 ± 0.02	0.04 ± 0.03	83 900	5100
	CL	642	658	379	883	721	1.19×10^5	0.75 ± 0.01	0.06 ± 0.01	88 800	7300
5f	TOL	653	669	367	915	696	1.18×10^5	0.71 ± 0.01	0.01 ± 0.01	83,100	1300
	CL	648	667	440	988	773	1.06×10^5	0.70 ± 0.01	0.02 ± 0.01	74 200	2000

^a All values are averaged over three independent measurements. ^b Spectrograde solvents were used for all measurements; TOL = toluene, CL = chloroform. ^c Absorption maximum. ^d Fluorescence emission maximum. ^e Energy difference between the absorption and emission maxima. ^f Full-width-at-half-maximum of the absorption band. ^g Full-width-at-half-maximum of the emission band. ^h Molar attenuation coefficient. ⁱ Fluorescence quantum yield determined vs. Nile blue ($\Phi_f = 0.27$, $\lambda_{\text{exc}} = 605$ nm in spectrograde ethanol). Standard deviations are reported. ^j Singlet oxygen quantum yield determined vs. methylene blue ($\Phi_{\Delta} = 0.52$, $\lambda_{\text{exc}} = 639$ nm in spectrograde ethanol) by monitoring the absorbance of 1,3-DPBF at 414 nm. Standard deviations are reported. ^k Fluorescence brightness. ^l Phototoxic power.

substituent, albeit being bent out of plane (Fig. S11, ESI[†]). This conformer is henceforth termed the 'coplanar' conformer for convenience. (TD)DFT calculations were repeated for this conformer and are presented in Tables S4, S5 and Fig. S12 (ESI[†]). We observed a slightly lower S₁ state compared to the perpendicular conformer (Table 1), providing a possible explanation for the presence of the red absorption shoulder for **5c** in Fig. 2. Despite the larger calculated oscillator strength for the coplanar conformer, this red-shifted absorption is, however, of lower intensity. In addition, the coplanar conformer is not observed in the single-crystal structure and therefore it is considered to be less present and of little importance for the further discussion.

For the six BODIPY dyes, the emission maxima are close to their absorption counterparts, resulting in small Stokes shifts, both in chloroform and toluene solution. For phenothiazine-BODIPY dyad **5c**, the difference between the absorption and emission maxima reaches 50 nm in chloroform. This large offset is of interest for future PDT applications, since it limits interference between the activation light and the emitted fluorescence. For BODIPYs **5b**, **c**, only one (strongly tailing) fluorescence peak is seen. For the other donors **5a**, **d–f**, a low-energy emission shoulder of varying relative intensity is noticed. For a better visualization of the spectroscopic differences within the complete series, the absorption and emission profiles were plotted together in a separate figure for each solvent in Fig. S13 (ESI[†]).

Φ_f and Φ_{Δ} values depend on the type of donor introduced and differ significantly. Generally, the fluorescence ability decreases compared to BODIPY precursor **2** ($\Phi_f = 0.97$ in dichloromethane),⁷⁵ as expected for red-shifted dyes due to the energy-gap law. However, these values are still significant, retaining a Φ_f of at least 40% in chloroform as well as in toluene solution for dyads **5a**, **d–f**. The brightest variants are obtained with dimethylacridine (**5a**), carbazole (**5e**), and di-*tert*-butylcarbazole (**5f**) donors, with quantum yields around 70%.

BODIPYs **5b**, **c** are somewhat peculiar as their emission is almost negligible in chloroform, but close to 50% in toluene. According to Φ_{Δ} , we can divide the six dyads into two groups, in line with our observations on the D–A dihedral angles given in Fig. 1. The BODIPY materials based on diphenylamine and both carbazole donors (**5d–f**; $\theta_{\text{D–A}} < 90^\circ$) are unable to produce a considerable amount of ¹O₂ during excitation at 639 nm (around or below 6%). On the other hand, dimethylacridine, phenoxazine, and phenothiazine (**5a–c**; $\theta_{\text{D–A}} = 90^\circ$) afford suitable PSs with ¹O₂ quantum yields of 23, 37, and 38% in chloroform, respectively. The Φ_{Δ} value for the dimethylacridine-based dyad **5a** in toluene drops below 10%. Interestingly, this is not the case for phenoxazine and phenothiazine dyads **5b–c**, where ¹O₂ production is still significant, with yields of 47 and 33%, respectively. Hence, the combination of strong fluorescence and ¹O₂ formation, together with their high molar attenuation coefficients, renders these new distyryl-BODIPY dyes promising dual-functioning PSs.

Solvent- and concentration-dependent fluorescence

At this stage, the underlying mechanism explaining the differences in Φ_{Δ} remains unclear. TDDFT calculations (Table 2) showed that ISC *via* intermediate CT states (SOCT-ISC), as often proposed in literature for push–pull type (BODIPY) dyes, seems unlikely as there is no available CT state.^{40–42,47,48} The presence of CT states can be revealed photophysically by evaluating the fluorescence profiles in solvents of different polarity. As CT states are highly polar excited states, a polar medium stabilizes these. Hence, CT bands typically display a bathochromic shift in polar solvents. Furthermore, CT bands initially absent in a apolar solvent can be revealed in polar medium as the CT state might become more populated and/or emissive relaxation toward the ground state is favored as a result of the changed CT energy. Additional measurements were hence performed in the more polar solvents acetone, dimethyl sulfoxide (DMSO), and acetonitrile (Fig. S9, S13–S14 and Tables S3, S6, ESI[†]). For

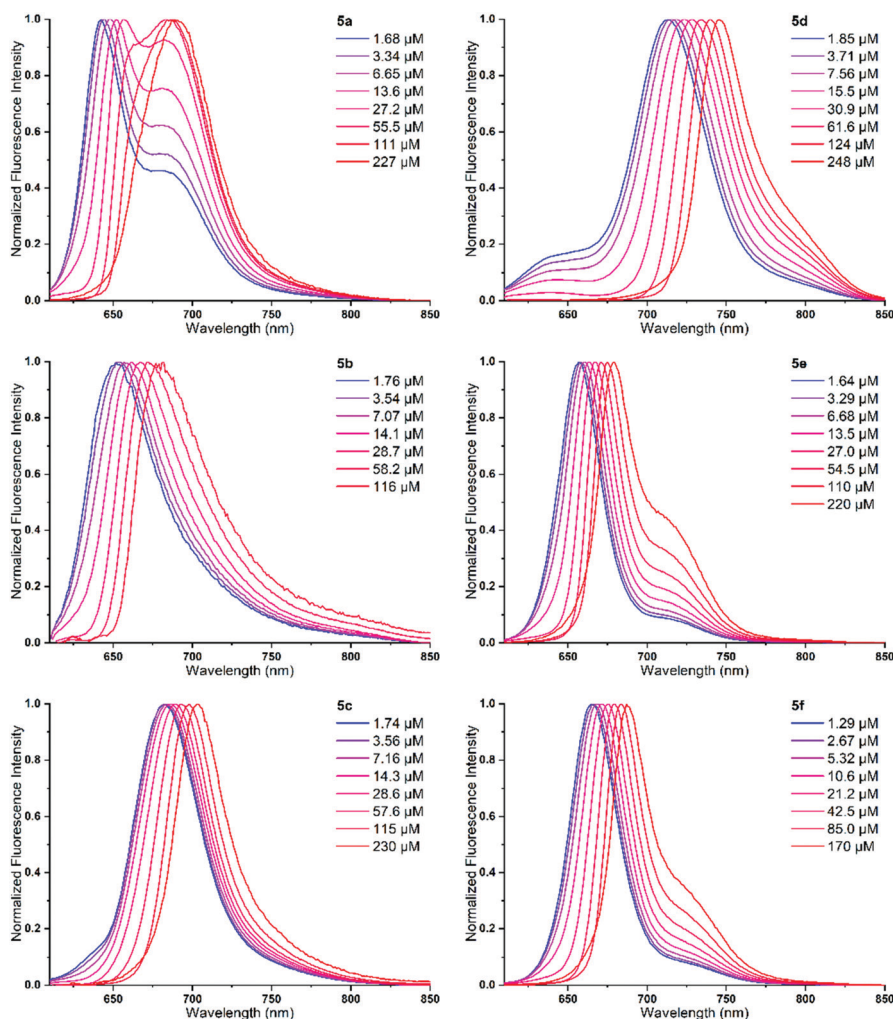


Fig. 3 Normalized fluorescence emission spectra for a dilution series of BODIPYs **5a–f** in chloroform ($\lambda_{\text{exc}} = 605 \text{ nm}$).

dyads **5d–f**, no meaningful influence of solvent polarity on the emission profile was observed. The fluorescence of BODIPYs **5a–c** did vary to some extent between polar and apolar solvents. For the dyads with phenoxazine (**5b**) and phenothiazine (**5c**), a potential CT band can be distinguished. However, the nearly completely quenched fluorescence in **5a–c** (Table S6, ESI[†]) renders these observations rather inconclusive.

In our previous work on BODIPY-dimethylacridine dyads (**5a**), we suggested that ISC could possibly proceed *via* an exciplex intermediate state (¹EX).⁶⁶ Hence, a similar screening of the fluorescence profile at different concentrations was performed for BODIPYs **5b–f** (Fig. 3 and Fig. S15–S17, ESI[†]).

A bathochromic shift in the fluorescence maxima was observed for the six BODIPYs upon increasing concentration. This is a commonly observed phenomenon, whereby the increased molecular interaction enlarges the perceived Stokes shift (inner filter effect).⁷⁶ As previously described, dyad **5a** shows a strong increase in relative intensity of a second emission band as the concentration increases.⁶⁶ In diluted samples, the localized singlet state (¹LE) emission at 645 nm is most intense. As concentration increases, the relative

population of the ¹LE and ¹EX band is altered, and the exciplex state becomes more distinct. This trend results in an exciplex band ($\lambda_{\text{em,EX}} = 690 \text{ nm}$) that transcends the ¹LE emission. At high concentration, the ¹LE emission even disappeared completely, with only the emission from the ¹EX state remaining. Similar behavior is observed in toluene (Fig. S14, ESI[†]). For the other dyads (**5b–f**), this remarkable behavior is not explicitly visible (Fig. 3 and Fig. S15, ESI[†]). A slight increase of the long-wavelength fluorescence shoulder can be noticed for BODIPYs **5d–f** upon increasing concentration, but not at all to the same extent as for **5a**. Furthermore, the dyads with phenoxazine and phenothiazine donors (**5b–c**) do not show a second emission band resulting from molecular aggregation, despite their ISC ability. Hence, exciplex formation seems to occur only for dyad **5a**, whereas BODIPYs **5b–c** have to rely on another mechanism to explain their high ¹O₂ generation capabilities upon photoexcitation. To get a better idea of the relative fluorescence intensities at different concentrations, these data were also normalized to the concentration (Fig. S16 and S17, ESI[†]). In all cases, a strong quenching of the emissive behavior was observed upon increasing concentration.

1 Femtosecond transient absorption spectroscopy

Transient absorption spectra, achieved with a high time resolution of ~ 30 fs, were recorded to gain additional information on the ultrafast excited state evolutions of the dyads. All samples were excited using a broadband ultrashort pulse (< 30 fs) covering the 550–760 nm spectral range. A second broadband ultrashort pulse was used as the probe beam. Transient spectra were acquired within a pump–probe time delay window of 200 ps. The raw transient absorption spectra are shown in Fig. S18 and S19 (ESI[†]). To extract the time constants associated with the excited state evolution, a global fitting of the kinetic traces was performed using a sequential linear kinetic scheme (using the software Glotaran).⁷⁷ The evolution-associated difference spectra (EADS) obtained from global analysis for BODIPYs **5a–f** in toluene solution are reported in Fig. 4. Global analysis was also performed on the transient data of dyads **5a–f** in chloroform solution (Fig. S20, ESI[†]). The EADS are very similar to those obtained in toluene solution, although there are small differences in the extracted kinetic constants. To facilitate the

analysis of the new dyads, a reference compound lacking a donor moiety (distyryl-BODIPY **5H**, donor = H in Scheme 1) was synthesized and transient spectra were acquired for this compound as well (see Fig. S21 and the associated discussion in the ESI[†]).

Considering the newly synthesized dyads **5a–f**, whose EADS are reported in Fig. 4, the most intense signal is a negative band whose position matches well with the absorption maximum (Fig. 2) and can thus be assigned to ground-state bleaching (GSB). Besides, differences are observed for the smaller intensity excited-state absorption (ESA) and stimulated emission (SE) bands. As noticed in Fig. 4, the EADS of BODIPYs **5b, c** are qualitatively similar. In both cases, a positive band is observed to rise on a 10–20 ps timescale in the 680–750 nm region, while the low intensity SE band is not observed for these systems. In case of phenoxazine-BODIPY **5b**, the positive signal starts rising at the short timescale since it is already observed in the second spectral component, with a rise time of 200 fs. The positive band is initially peaked at 700 nm. Within the following 5.5 ps, the ESA intensity increases and a second maximum at 730 nm

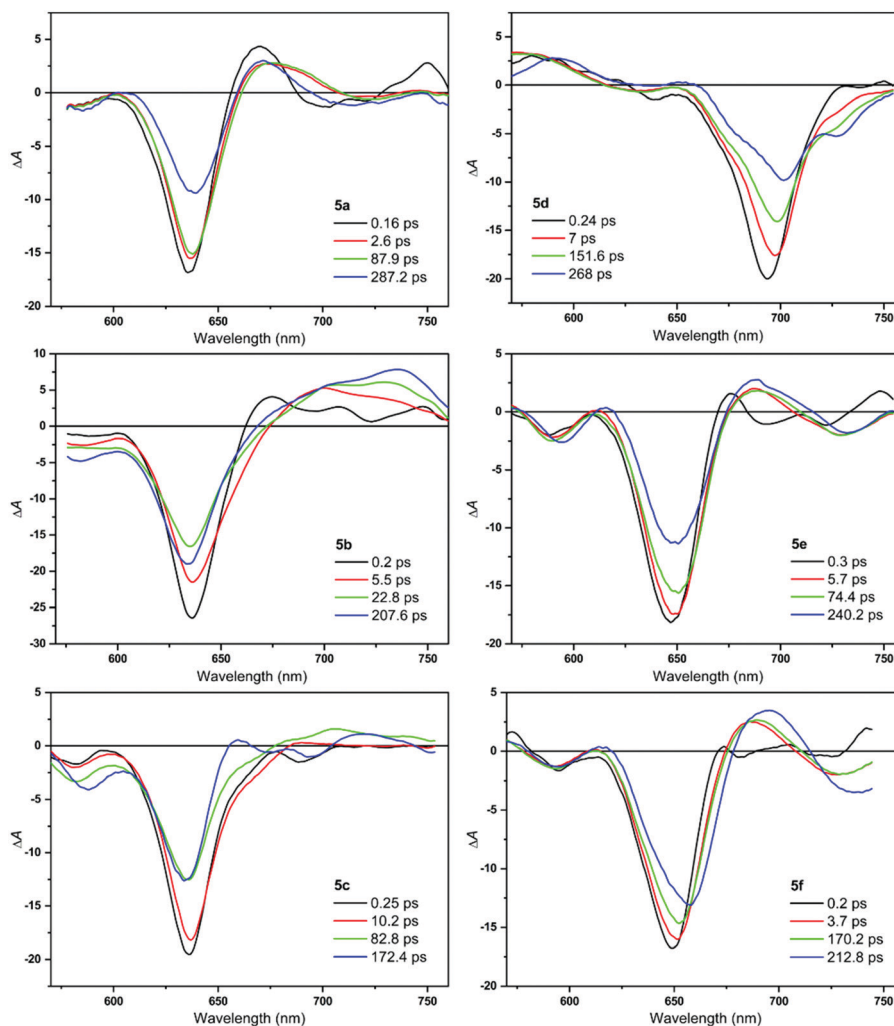


Fig. 4 Evolution-associated difference spectra (EADS) for BODIPYs **5a–f** in toluene solution as obtained by singular value decomposition (SVD) and global fitting of the transient data (target analysis).

1 appears. The band further rises in the evolution toward the
following EADS, occurring in 23 ps. The intensity of the
bleaching signal progressively recovers, and its peak slightly
blue-shifts in time. For phenothiazine-BODIPY **5c**, the rise of
5 the positive band appears slower as compared to **5b**. Indeed, a
positive band peaked at 700 nm is clearly observed only in the
third spectral component, rising in 10 ps. In the following
EADS, a negative signal appears in the 660–700 nm region,
10 while two positive peaks are visible at 650 and 710 nm. The
appearance of a positive band on the red side of the bleaching
band can point to the occurrence of charge separation between
the BODIPY core and the donor substituents. Indeed, it was
previously indicated that the localization of a negative charge
15 on the BODIPY core induces the appearance of an absorption
band on the red side of the GSB of the correspondent neutral
species.^{64,78–80} The spectral evolution observed for dyad **5c** on
the 83 ps timescale could point to a structural relaxation of the
charge-separated state (CSS).

The occurrence of charge separation is less clear in case of
20 BODIPY **5a**. The transient spectra registered in the two solvents
are very similar (Fig. 4 and Fig. S20, ESI[†]). The initial EADS
resembles that of the distyryl BODIPY without a donor moiety
(**5H**; Fig. S21, ESI[†]). The signal evolves in 160 fs, with the ESA
band broadening and compensating the SE band. The spectral
25 shape remains almost unvaried in the following evolution (2.6
ps), while in the subsequent evolution (88 ps) both the GSB and
ESA band decrease in intensity. A small SE signal is again
visible in the final spectral component because of the
decreased intensity of the positive signal in the same region.
30 The rise of a positive signal in the 700 nm region could indicate
the presence of a CSS. However, the kinetics of this process are
different compared to what was observed for BODIPYs **5b**, **c**.
Comparing the kinetic traces recorded on the ESA band of
compounds **5a–c** (Fig. S22, ESI[†]), it can be noticed that the
35 positive band in **5b**, **c** rises on a similar timescale of a few tens
of ps, while the rise for **5a** is much faster and is followed by a
faster decay. Comparison of the transient absorption data thus
suggests that the ISC mechanism for these dyes might be
different, with triplet formation possibly mediated by the
40 presence of exciplexes in case of dimethylacridine-BODIPY **5a**
and charge separation/recombination for phenoxazine- and
phenothiazine-BODIPYs **5b**, **c**.

The EADS of BODIPYs **5d–f** are qualitatively different from
those of BODIPYs **5a–c** (Fig. 4 and Fig. S20, ESI[†]). In particular,
45 the EADS of carbazole-BODIPYs **5e**, **f** closely resemble those of
the distyryl-BODIPY **5H**, although red-shifted. The ESAs
observed in these compounds, peaked at 688 and 700 nm,
respectively, have a very fast rise, suggesting that this signal is
associated to the bright S₁ state. This is clearly shown by the
50 comparison of the kinetic traces recorded on the ESAs of **5b** and
5f shown in Fig. S23 (ESI[†]). The spectra of diphenylamine-
BODIPY **5d** are different, reflecting the strong red-shift in the
absorption observed for this sample. Indeed, in this case, the
bleaching signal is located at 693 nm and an ESA band is
55 observed in the blue part of the investigated spectral region
(560 nm). Following the time evolution, the bleaching

progressively recovers, while a SE band appears around
730 nm. This band progressively increases in intensity and
slightly red-shifts, signaling the occurrence of emission by a
relaxed excited state. Nevertheless, also in this case there is no
5 indication of the involvement of other excited states in the
dynamics, which thus proceeds through relaxation from the
bright S₁ state.

To gain additional information on the occurrence of charge
separation and the differences observed in dyads **5a–c** as
compared to **5d–f**, transient spectra of two representative
10 compounds for each group, namely **5b** and **5e**, were measured
on an extended timescale reaching 1.5 ns pump–probe delay.
The EADS obtained by performing a global analysis on these
data, in both chloroform and toluene, are reported in the
supplementary information (Fig. S24 and S25 (ESI[†]) and related
15 comments). By inspection of the EADS, it can be noticed that
the excited state dynamics on the timescale >200 ps are highly
influenced by solvent polarity in case of BODIPY **5b**, as is
expected in case of charge separation. Indeed, the transient
spectra recover almost completely within the 1.5 ns timescale in
20 chloroform, suggesting the occurrence of charge recombina-
tion, while slower dynamics are observed in toluene. In case of
5e, both the spectral shape and the signal evolution are almost
independent on solvent polarity.

Excited state geometry optimizations

Since the femtosecond transient absorption spectra suggest the
presence of an intermediate state with CT character in BODIPY
dyads **5b**, **c** (Fig. 4), whereas there is no evidence of the
involvement of this state from TDDFT calculations on the
30 ground state geometry (Table 2), excited state geometry opti-
mizations were performed to probe the effects of geometrical
relaxation. While higher level methods such as *riCC2* or
CASPT2 are preferred to optimize the excited state geometries
of molecules exhibiting CT character, it has been shown that
35 XC functionals with significant amounts of Hartree–Fock
exchange, such as *M06-2X* or long-range corrected XC func-
tionals such as *CAM-B3LYP*, give reasonable results with
respect to these higher level methods or experimental
results.^{81–83} Since higher level methods (*riCC2*, *CASPT2*, *etc.*)
40 are too computationally demanding for these molecules, the
same level of approximation as applied for the ground state
optimizations (*M062X/6-311G(d)*) was used. The excited state
geometries for the first (LE character) and second (CT char-
acter) excited states were optimized in the gas phase. Upon
45 relaxation, the first singlet excited states of BODIPYs **5a**, **b** show
smaller D–A dihedral angles of 82° and 64°, respectively (Fig.
S26 and S27, ESI[†]). For BODIPY **5c**, this is not the case (Fig. S28,
ESI[†]). BODIPYs **5d–f** do not show significant differences in the
D–A dihedral angles as compared to the ground states either
50 (Fig. S29–S31, ESI[†]). The decrease in dihedral angle for **5a**, **b**
leads to a delocalization of the HOMO onto the donor and
distyryl-BODIPY fragments and mixes CT and LE character for
the first singlet excited state (Fig. S26, S27 and Table S7, ESI[†]).
For **5b**, this effect is much stronger due to the strongly reduced
55 dihedral angle with respect to the ground state geometry. When

1 optimizing the second singlet excited state, the D–A dihedral
angles remain unchanged as compared to the ground state (Fig.
S26–S31, ESI†). The S_1 – S_2 energy difference ($\Delta E_{S_1-S_2}$) remains
5 unchanged for BODIPYs **5d–f** and no mixing of CT and LE
character is observed for these molecules. However, a strong
decrease of $\Delta E_{S_1-S_2}$ is observed for BODIPYs **5a** and (in parti-
cular) **5b**, indicating that the excited states are close in energy
for this given geometry (Table S8, ESI†). For dyad **5c**, we were
10 unable to optimize the second singlet excited state due to a
rearrangement of the energy levels during the optimization
procedure. We do observe that the vertical de-excitation ener-
gies of S_1 and S_2 come very close and even invert before the
energy level rearrangement occurs. These results indicate that
15 after excited state relaxation, the LE and CT excited state come
closer in energy for BODIPYs **5b, c** thus enabling a mixing
between them. This is in line with the findings of the femto-
second transient absorption experiments and further solidifies
the hypothesis that a CT state is involved in the ISC process.

Involvement of CT states also allows to clarify the strong
20 solvent dependence of the fluorescence intensity of **5b, c**
(Table 3). As CT states are highly polar excited states, their
energy is strongly affected by the surrounding medium.⁸⁴ In a
more polar solvent (*e.g.* chloroform), the CT state is stabilized,
thereby decreasing its energy. However, the approach of the CT
25 state to the ground state induces more radiationless relaxation.
Accordingly, dyads **5b, c** show quenched emission in chloro-
form. In relatively apolar toluene solution, a larger singlet state
population is retained, preserving the fluorescence.

30 Conclusions

A series of six different distyryl–BODIPY–donor dyads were
35 synthesized and the photophysical properties were evaluated
with an eye on their potential application as photosensitizers in
image-guided photodynamic therapy. All dyes show strong
absorption in the phototherapeutic window. The main differ-
ences are found in their brightness and phototoxic behavior.
BODIPYs bearing diphenylamine or carbazole donors show
40 moderate to strong fluorescence, respectively, but produce very
little singlet oxygen upon photoexcitation. Dimethylacridine,
phenoxazine, and phenothiazine donors are oriented perpen-
dicularly with respect to the styryl moieties in the ground state
geometry. This seems to be an essential structural feature as,
45 next to a moderate fluorescence quantum yield, these dyads
afford significant singlet oxygen quantum yields without the
aid of heavy atoms. Phenoxazine- and phenothiazine-bearing
BODIPYs show improved photosensitizer characteristics with
respect to the earlier reported dimethylacridine–distyryl BOD-
50 IPY dyads. With $\Phi_f = 53\%$ and $\Phi_\Delta = 33\%$ for phenothiazine, and
 $\Phi_f = \Phi_\Delta = 47\%$ for phenoxazine (in toluene), these new dyads
can be considered as highly promising dual-functioning photo-
sensitizers. The intersystem crossing mechanism in the BOD-
IPY dyads was studied using femtosecond transient absorption
55 spectroscopy. Charge separation/recombination seems to take
place in the phenoxazine- and phenothiazine-based molecules.

This hypothesis was further solidified by optimizing the first
1 and second excited state geometries, revealing their relatively
small energy difference, allowing mixing between them.
Further improvements with respect to the donor could be
5 explored toward even more efficient BODIPY photosensitizers.
However, one should be aware that several other factors come
into play besides merely donor strength. Although a new donor
could improve charge-transfer characteristics, other variables
(*e.g.* geometry, redox potential, dipole moment, charge recom-
10 bination) will change as well, thereby affecting the overall
phototoxicity. Balancing these effects remains the key toward
high-performance dual photosensitizers. In any case, due to the
promising results for our present donor–acceptor BODIPY
dyads, further steps will already be taken to probe their
15 behavior in biological media with an eye on future *in vitro*
and *in vivo* examinations.

Conflicts of interest

There are no conflicts of interest to declare. 20

Acknowledgements

The authors thank Hasselt University and the University of
25 Namur for continuing financial support (PhD scholarships JD
and TC). BC and WM thank the Research Foundation – Flan-
ders (FWO) for support through projects G087718N,
G0D1521N, I006320N, GOH3816NAUHL, and the Scientific
Research Community ‘Supramolecular Chemistry and Materi-
30 als’ (W000620N). The calculations were performed on the
computers of the ‘Consortium des équipements de Calcul
Intensif (CÉCI)’ (<http://www.cecii-hpc.be>), including those of
the ‘UNamur Technological Platform of High-Performance
Computing (PTCI)’ (<http://www.ptci.unamur.be>), for which we
35 gratefully acknowledge financial support from the FNRS-FRFC,
the Walloon Region, and the University of Namur (Conventions
no. 2.5020.11, GEQ U.G006.15, U.G018.19, 1610468, and RW/
GEQ2016). SD, AL, and MDD acknowledge support from the
European Union’s Horizon 2020 research and innovation pro-
40 gram under grant agreement no. 871124 Laserlab-Europe. Q4

References

- 1 M. C. DeRosa and R. J. Crutchley, *Coord. Chem. Rev.*, 2002, **233**, 351–371. 45
- 2 J. Moan, *J. Photochem. Photobiol., B*, 1990, **6**, 343–347.
- 3 J. Moan and K. Berg, *Photochem. Photobiol.*, 1991, **53**, 549–553.
- 4 S. Kwiatkowski, B. Knap, D. Przystupski, J. Saczko, E. Kedzierska, K. Knap-Czop, J. Kotlinska, O. Michel, K. Kotowski and J. Kulbacka, *Biomed. Pharmacother.*, 2018, **106**, 1098–1107. 50
- 5 H. I. Pass, *J. Natl. Cancer Inst.*, 1993, **85**, 443–456.
- 6 W. M. Sharman, C. M. Allen and J. E. van Lier, *Drug* 55 *Discovery Today*, 1999, **4**, 507–517.

- 1 7 T. J. Dougherty, *J. Clin. Laser Med. Sur.*, 2002, **20**, 3–7.
- 8 M. R. Hamblin and T. Hasan, *Photochem. Photobiol. Sci.*, 2004, **3**, 436–450.
- 9 Z. Huang, *Technol. Cancer Res. Treat.*, 2005, **4**, 283–293.
- 5 10 M. A. MacCormack, *Semin. Cutaneous Med. Surg.*, 2008, **27**, 52–62.
- 11 P. Babilas, S. Schreml, M. Landthaler and R. M. Szeimies, *Photodermatol., Photoimmunol. Photomed.*, 2010, **26**, 118–132.
- 10 12 T. Dai, B. B. Fuchs, J. J. Coleman, R. A. Prates, C. Astrakas, T. G. Denis, M. S. Ribeiro, E. Mylonakis, M. R. Hamblin and G. P. Tegos, *Front. Microbiol.*, 2012, **3**, 120–136.
- 13 C. S. Foote, *Photochem. Photobiol.*, 1991, **54**, 659.
- 14 A. P. Castano, T. N. Demidova and M. R. Hamblin, *Photo-diagn. Photodyn. Ther.*, 2004, **1**, 279–293.
- 15 15 V. Kral, J. Davis, A. Andrievsky, J. Kralova, A. Synytsya, P. Pouckova and J. L. Sessler, *J. Med. Chem.*, 2002, **45**, 1073–1078.
- 16 S. J. Wagner, *Transfus. Med. Rev.*, 2002, **16**, 61–66.
- 20 17 R. R. Allison, G. H. Downie, R. Cuenca, X. H. Hu, C. J. Childs and C. H. Sibata, *Photodiagn. Photodyn. Ther.*, 2004, **1**, 27–42.
- 18 M. R. Detty, S. L. Gibson and S. J. Wagner, *J. Med. Chem.*, 2004, **47**, 3897–3915.
- 25 19 A. E. O'Connor, W. M. Gallagher and A. T. Byrne, *Photochem. Photobiol.*, 2009, **85**, 1053–1074.
- 20 S. Swavey and M. Tran, in *Recent Advances in the Biology, Therapy and Management of Melanoma*, ed. L. Davids, IntechOpen, London, 2013, ch. 11, pp. 254–282.
- 30 21 R. D. Teo, J. Y. Hwang, J. Termini, Z. Gross and H. B. Gray, *Chem. Rev.*, 2017, **117**, 2711–2729.
- 22 S. D'Alessandro and R. Prierer, *J. Drug Delivery Sci. Technol.*, 2020, **60**, 101979.
- 23 J. Deckers, T. Cardeynaels, L. Lutsen, B. Champagne and W. Maes, *Chem. Phys. Chem.*, 2021, **22**, 1488–1496.
- 35 24 S. G. Awuah and Y. You, *RSC Adv.*, 2012, **2**, 11169–11183.
- 25 L. Yao, S. Z. Xiao and F. J. Dan, *J. Chem.*, 2013, 1–10.
- 26 A. Kamkaew, S. H. Lim, H. B. Lee, L. V. Kiew, L. Y. Chung and K. Burgess, *Chem. Soc. Rev.*, 2013, **42**, 77–88.
- 40 27 C. S. Kue, S. Y. Ng, S. H. Voon, A. Kamkaew, L. Y. Chung, L. V. Kiew and H. B. Lee, *Photochem. Photobiol. Sci.*, 2018, **17**, 1691–1708.
- 28 L. Huang and G. Han, *Small Methods*, 2018, **2**, 1700370.
- 29 A. Turksoy, D. Yildiz and E. U. Akkaya, *Coord. Chem. Rev.*, 2019, **379**, 47–64.
- 45 30 W. Sun, X. Zhao, J. Fan, J. Du and X. Peng, *Small*, 2019, **15**, 1804927.
- 31 M. L. Agazzi, M. B. Ballatore, A. M. Durantini, E. N. Durantini and A. C. Tomé, *J. Photochem. Photobiol., C*, 2019, **40**, 21–48.
- 50 32 D. Chen, Z. Zhong, Q. Ma, J. Shao, W. Huang and X. Dong, *ACS Appl. Mater. Interfaces*, 2020, **12**, 26914–26925.
- 33 P. Chinna Ayya Swamy, G. Sivaraman, R. N. Priyanka, S. O. Raja, K. Ponnuvel, J. Shanmugpriya and A. Gulyani, *Coord. Chem. Rev.*, 2020, **411**, 213233.
- 55 34 W. Lin, D. Colombani-Garay, L. Huang, C. Duan and G. Han, *WIREs Nanomed. Nanobiotechnol.*, 2020, **12**, 1627.
- 35 R. Prieto-Montero, A. Prieto-Castañeda, R. Sola-Llano, A. R. Agarrabeitia, D. Garcia-Fresnadillo, I. López-Arbeloa, A. Villanueva, M. J. Ortiz, S. de la Moya and V. Martínez-Martínez, *Photochem. Photobiol.*, 2020, **96**, 458–477.
- 5 36 W. Zhang, A. Ahmed, H. Cong, S. Wang, Y. Shen and B. Yu, *Dyes Pigm.*, 2021, **185**, 108937.
- 37 A. Loudet and K. Burgess, *Chem. Rev.*, 2007, **107**, 4891–4932.
- 38 G. Ulrich, R. Ziessel and A. Harriman, *Angew. Chem., Int. Ed.*, 2008, **47**, 1184–1201.
- 39 N. Boens, B. Verbelen and W. Dehaen, *Eur. J. Org. Chem.*, 2015, 6577–6595.
- 40 J. Zhao, K. Xu, W. Yang, Z. Wang and F. Zhong, *Chem. Soc. Rev.*, 2015, **44**, 8904–8939.
- 15 41 K. Chen, Y. Dong, X. Zhao, M. Imran, G. Tang, J. Zhao and Q. Liu, *Front. Chem.*, 2019, **7**, 1–14.
- 42 J. Wang, Q. B. Gong, L. Wang, E. H. Hao and L. J. Jiao, *J. Porphyrins Phthalocyanines*, 2020, **24**, 603–635.
- 43 G. Kubheka, B. Babu, E. Prinsloo, N. Kobayashi, J. Mack and T. Nyokong, *J. Porphyrins Phthalocyanines*, 2020, **25**, 47–55.
- 20 44 J. Zhao, W. Wu, J. Sun and S. Guo, *Chem. Soc. Rev.*, 2013, **42**, 5323–5351.
- 45 J. Zhao, K. Chen, Y. Hou, Y. Che, L. Liu and D. Jia, *Org. Biomol. Chem.*, 2018, **16**, 3692–3701.
- 25 46 Y. Hou, X. Zhang, K. Chen, D. Liu, Z. Wang, Q. Liu, J. Zhao and A. Barbon, *J. Mater. Chem. C*, 2019, **7**, 12048–12074.
- 47 M. A. Filatov, *Org. Biomol. Chem.*, 2020, **18**, 10–27.
- 48 V. N. Nguyen, Y. Yan, J. Zhao and J. Yoon, *Acc. Chem. Res.*, 2021, **54**, 207–220.
- 30 49 J. P. Celli, B. Q. Spring, I. Rizvi, C. L. Evans, K. S. Samkoe, S. Verma, B. W. Pogue and T. Hasan, *Chem. Rev.*, 2010, **110**, 2795–2838.
- 50 S. S. Kelkar and T. M. Reineke, *Bioconjugate Chem.*, 2011, **22**, 1879–1903.
- 35 51 X. Chen and S. T. C. Wong, *Cancer Theranostics*, Academic Press, Oxford, 2014.
- 52 T. J. Dougherty and S. L. Marcus, *Eur. J. Cancer*, 1992, **28**, 1734–1742.
- 53 K. Plaetzer, B. Krammer, J. Berlanda, F. Berr and T. Kiesslich, *Lasers Med. Sci.*, 2009, **24**, 259–268.
- 40 54 K. Deng, C. Li, S. Huang, B. Xing, D. Jin, Q. Zeng, Z. Hou and J. Lin, *Small*, 2017, **13**, 1702299.
- 55 A. B. Descalzo, H. J. Xu, Z. Shen and K. Rurack, *Ann. N. Y. Acad. Sci.*, 2008, **1130**, 164–171.
- 45 56 L. Yuan, W. Lin, K. Zheng, L. He and W. Huang, *Chem. Soc. Rev.*, 2013, **42**, 622–661.
- 57 Y. Ni and J. Wu, *Org. Biomol. Chem.*, 2014, **12**, 3774–3791.
- 58 H. Lu, J. Mack, Y. Yang and Z. Shen, *Chem. Soc. Rev.*, 2014, **43**, 4778–4823.
- 50 59 S. G. Awuah, S. K. Das, F. D'Souza and Y. You, *Chem. – Asian J.*, 2013, **8**, 3123–3132.
- 60 R. L. Watley, S. G. Awuah, M. Bio, R. Cantu, H. B. Gobeze, V. N. Nesterov, S. K. Das, F. D'Souza and Y. You, *Chem. – Asian J.*, 2015, **10**, 1335–1343.
- 55

- 1 61 Z. Wang, L. Huang, Y. Yan, A. M. El-Zohry, A. Toffoletti, J. Zhao, A. Barbon, B. Dick, O. F. Mohammed and G. Han, *Angew. Chem., Int. Ed.*, 2020, **59**, 16114–16121.
- 62 H. Ito, H. Sakai, Y. Suzuki, J. Kawamata and T. Hasobe, *Chem. – Eur. J.*, 2020, **26**, 316–325.
- 5 63 Y. Hou, Q. Liu and J. Zhao, *Chem. Commun.*, 2020, **56**, 1721–1724.
- 64 Y. Dong, A. Elmali, J. Zhao, B. Dick and A. Karatay, *Chem. Phys. Chem.*, 2020, **21**, 1388–1401.
- 10 65 G. Turkoglu, G. Kayadibi Koygun, M. N. Z. Yurt, N. Demirok and S. Erbas-Cakmak, *Org. Biomol. Chem.*, 2020, **18**, 9433–9437.
- 66 J. Deckers, T. Cardeynaels, H. Penxten, A. Ethirajan, M. Ameloot, M. Kruk, B. Champagne and W. Maes, *Chem. – Eur. J.*, 2020, **26**, 15212–15225.
- 15 67 As the exact structure of these ‘exciplexes’ (*i.e.* excited state complexes) remains unknown for now, we propose to use this more general term.
- 68 A. C. Benniston, G. Copley, H. Lemmetyinen and N. V. Tkachenko, *Chem. Phys. Chem.*, 2010, **11**, 1685–1692.
- 20 69 A. C. Benniston, A. Harriman, V. L. Whittle, M. Zelzer, R. W. Harrington and W. Clegg, *Photochem. Photobiol. Sci.*, 2010, **9**, 1009–1017.
- 70 A. Nano, R. Ziessel, P. Stachelek, M. A. Alamiry and A. Harriman, *Chem. Phys. Chem.*, 2014, **15**, 177–186.
- 25 71 Y. Rong, C. Wu, J. Yu, X. Zhang, F. Ye, M. Zeigler, M. E. Gallina, I. C. Wu, Y. Zhang, Y. H. Chan, W. Sun, K. Uvdal and D. T. Chiu, *ACS Nano*, 2013, **7**, 376–384.
- 72 H. Y. Yang, M. Zhang, J. W. Zhao, C. P. Pu, H. Lin, S. L. Tao, C. J. Zheng and X. H. Zhang, *Chin. J. Chem.*, 2021, **39**.
- 73 T. Le Bahers, C. Adamo and I. Ciofini, *J. Chem. Theory Comput.*, 2011, **7**, 2498–2506.
- 74 K. Wang, Y. Z. Shi, C. J. Zheng, W. Liu, K. Liang, X. Li, M. Zhang, H. Lin, S. L. Tao, C. S. Lee, X. M. Ou and X. H. Zhang, *ACS Appl. Mater. Interfaces*, 2018, **10**, 31515–31525.
- 5 75 A. B. Nepomnyashchii, M. Broring, J. Ahrens and A. J. Bard, *J. Am. Chem. Soc.*, 2011, **133**, 8633–8645.
- 76 J. R. Lakowicz, *Principles of Fluorescence Spectroscopy*, Springer, Boston, MA, 3 edn, 2006.
- 10 77 J. J. Snellenburg, S. P. Laptinok, R. Seger, K. M. Mullen and I. H. M. V. Stokkum, *J. Stat. Soft.*, 2012, **49**, 1–22.
- 78 Z. Mahmood, M. Taddei, N. Rehmat, L. Bussotti, S. Doria, Q. Guan, S. Ji, J. Zhao, M. Di Donato, Y. Huo and Y. H. Xing, *J. Phys. Chem. C*, 2020, **11**, 5944–5957.
- 15 79 Z. Wang, M. Ivanov, Y. Gao, L. Bussotti, P. Foggi, H. Zhang, N. Russo, B. Dick, J. Zhao, M. Di Donato, G. Mazzone, L. Luo and M. Fedin, *Chem. – Eur. J.*, 2020, **26**, 1091–1102.
- 80 M. A. Filatov, S. Karuthedath, P. M. Polestshuk, H. Savoie, K. J. Flanagan, C. Sy, E. Sitte, M. Telitchko, F. Laquai, R. W. Boyle and M. O. Senge, *J. Am. Chem. Soc.*, 2017, **139**, 6282–6285.
- 20 81 C. A. Guido, D. Jacquemin, C. Adamo and B. Mennucci, *J. Phys. Chem. A*, 2010, **114**, 13402–13410.
- 82 C. A. Guido, S. Knecht, J. Kongsted and B. Mennucci, *J. Chem. Theory Comput.*, 2013, **9**, 2209–2220.
- 25 83 D. Jacquemin, A. Planchat, C. Adamo and B. Mennucci, *J. Chem. Theory Comput.*, 2012, **8**, 2359–2372.
- 84 D. Escudero, *Acc. Chem. Res.*, 2016, **49**, 1816–1824.
- 30
- 35
- 40
- 45
- 50
- 55